Control of Spacecraft Formations Around the Libration Points Using Electric Motors with One Bit of Resolution

Edoardo Serpelloni[1], Manfredi Maggiore[1], and Christopher J. Damaren[2]

Abstract

This paper investigates a formation control problem for two space vehicles in the vicinity of the L_2 libration point of the Sun-Earth/Moon system. The objective is to accurately regulate the relative position vector between the vehicles to a desired configuration, under tight tolerances. It is shown that the formation control problem is solvable using six constant thrust electric actuators requiring only one bit of resolution, and bounded switching frequency. The proposed control law is hybrid, and it coordinates the sequence of on-off switches of the thrusters so as to achieve the control objective and, at the same time, avoid high-frequency switching.

I. Introduction

In recent years, several space agencies have proposed missions for the observation of the universe involving large spacecraft arrays flying in formation. The constraints imposed by the type of observations these missions must perform have led to the identification of trajectories in a neighborhood of the L_2 Lagrangian point of the Sun-Earth/Moon system as an ideal location. NASA proposed, in the context of the Vision Program, the Stellar Imager (SI) mission, a large array of nearly 30 spacecraft flying in formation to form a large telescope, see [1]. The Terrestrial Planet Finder (TPF) (see [2]) and the MAXIM mission concepts (see [3]) also involved large formations of spacecraft flying in the vicinity of the L_2 libration point (small baselines for TPF, very large for MAXIM).

These mission concepts share great challenges from the formation control perspective, as the relative position between spacecraft must be regulated with submillimetric error tolerances. In particular, SI requires the spacecraft to meet three different control specifications, classified as (see [1]): *rough control*, with accuracy up to a few meters; *intermediate control*, with accuracy of the order of a few centimeters; and, *fine control*, with submillimeter accuracy. Each of these control regimes is to be satisfied for an interval of time long enough to allow the scientific observation to be completed (for the SI mission, this would depend on the target star rotation period).

The formation control problem has been intensively studied in recent years. Discrete control methods, such as the Equitime Targeting Method ([4], [5]) and the Tangential Targeting Method

[1]E. Serpelloni and M. Maggiore are with the Electrical and Computer Engineering Department, University of Toronto, Toronto, ON, M5S 2J7, Canada. edoardo.serpelloni@scg.utoronto.ca, maggiore@ece.utoronto.ca.

[2]Christopher J. Damaren is with University of Toronto Institute for Aerospace Studies, Toronto, ON, M3H 5T6, Canada. damaren@utias.utoronto.ca

Preliminary versions of parts of this material have appeared in the conference proceedings [12], [13].

Published in *Journal of Astronautical Sciences, 2015*

[6], implement impulsive maneuvers at various checkpoints along the reference orbit in order to target a relative position Δr between leader and follower. However, these methods are not well suited for achieving accuracies at the subcentimeter level [4].
Howell *et al.* [4],[5], propose the application of Floquet control methods to formations in the vicinity of the reference Halo orbit in order to exploit the structure of the center manifold associated with the orbit itself. These techniques allow one to compute the maneuver required to initialize and keep the formation on the center manifold associated with the reference Halo orbit. The elements of the formation will evolve on a torus enveloping the nominal orbit, giving rise to quasi-periodic formations. By properly phasing each vehicle, the formation naturally evolves along the torus so that the relative positions of each spacecraft are unaltered and the relative distances are bounded.
The best performances are, however, guaranteed by the application of continuous control laws. The literature on continuous feedback control of formations is extensive, but very little of it is directly applicable to the problem at hand. Marchand and Howell in [7] explored the application of feedback linearization to the control of several different types of formations (aspherical, rigid, etc.). It is shown that the control of the elements of the formation can require thrust levels in the range $nN - mN$. In addition, the robustness of these methods to modeling errors and thrust implementation errors has yet to be explored. Gurfil and Kasdin, in [8], propose an optimal controller for a formation of two spacecraft, one of which is free flying along a natural trajectory of the Circular Restricted Three Body Problem (CR3BP). The controller is designed on a time-varying linearization of the CR3BP model about a natural solution. Such controllers require actuators with a dynamic range not achievable with today's technology. The authors of [8] recognize this limitation, and to overcome it they propose to mount different propulsive systems with different dynamic ranges. Gurfil *et al.* in [9] propose an approximate dynamic model inversion combined with linear compensation of the ideal feedback linearized model. Modeling errors and external perturbations are then compensated by a neural network element. Submillimetric tolerances are achieved, assuming thrusters providing continuous thrust in the mN-μN range. However, as pointed out in [4], [8] continuous control laws require the actuators to deliver thrust with prohibitively high resolution for today's technology. From a control perspective actuator resolution is, therefore, the crucial bottleneck in controlling spacecraft formations (of course in practice additional limitations arise from the accuracy of the measurements available to the spacecraft, this topic will not be addressed in this paper). Marchand and Stanton in [10], [11] have proposed to overcome such a limitation by using thrusters providing only a constant level of thrust. The control law they propose is based on the numerical solution of an optimization problem, where the on-off switching times for each of the on-board thrusters are the optimized variables.
In this paper, it is shown that the problem of controlling the relative position vector of two spacecraft flying in the vicinity of a libration point to any level of accuracy is solvable by implementing the controller presented in [12], [13] by the authors. It is assumed that the on-board thrusters can be either on or off, providing only a constant level of thrust (they deliver thrust with on-bit of resolution). The control law is intrinsically robust to all bounded perturbations acting on the spacecraft, provided that the propulsive system delivers enough thrust. Because of this property it is shown that the controller allows us to achieve the nominal control specifications in the full ephemerides system under the influence of additional, unmodeled external perturbations. The on-off switching function is designed for each thruster in order to meet virtually any level

of accuracy, while simultaneously avoiding high-frequency switching. FEEP (Field Emission Electric Propulsion) thrusters seem to best fit our requirements: they provide very low thrust (on the order of few μN) for long intervals of time and they are characterized by a fast turning on and turning off. The proposed control law is hybrid (the control input depends on the dynamics of a logic or discrete variable), and it only relies on the knowledge of the spacecraft relative position and relative velocity in body frame. No further parameters or measurements are required. The main advantage of the proposed controller is in that it completely overcomes the issue of thrusters' resolution that affects continuous controllers [4], [7],[8]. The second main advantage with respect to continuous controllers is in the ability to reject external disturbances. The issue of robustness has been explored in [8]. However, the continuous controller in [8] is robust only with respect to certain families of disturbances, modeled by means of an exogenous plant. The main limitation is that a precise model of the disturbances must be available in order to be replicated in the control law (see [8] for the details). This limitation is completely overcome by the controller proposed in the paper: we show that if a suitable set of thrusters is selected, the proposed controller meets the nominal control objectives even when the spacecraft are subject to unmodeled disturbances.
The proposed controller presents several advantages over the impulsive controllers in [4], [6]. First, strategies in [4], [6] are not well suited for enforcing tight tolerances because of technological limitations. Second of all, such controllers are open loop controllers, requiring an accurate knowledge of the system's model for planning and computing each maneuver. Moreover, the robustness properties of these control strategies have yet to be explored.
In the paper it is shown that the controller presented in [13] allows us to solve the formation control problem achiving two significant advantages over the controller presented in [10], [11]. First of all, the controller used in this paper is a feedback controller, that does not require any numerical procedure in order to compute the control value to be applied. Second of all, the controller implemented in this paper is intrinsically robust to modelling errors and external perturbations. This fact allows the controller to guarantee the achievement of the nominal control specifications in a wide variety of conditions.

The paper is organized as follows. Section II presents the equations of motion together with the problem statement and the control objectives. Section III presents the steps that led to the formulation of the proposed controller. The proposed controller is presented in Section IV. A robustness analysis with respect to attitude perturbations is presented in Section V. Simulations results are shown in Section VI.
Notation: In this paper the notations $(x_1,\dots,x_n)$ and $[x_1 \dots x_n]^T$ are used interchangeably to indicate vectors in $\mathbb{R}^n$. Given the vector $u = [u_1\ u_2\ u_3]^T \in \mathbb{R}^3$, $(\cdot)^\times$ denotes the skew symmetric matrix

$$u^\times = \begin{bmatrix} 0 & -u_3 & u_2 \\ u_3 & 0 & -u_1 \\ -u_2 & u_1 & 0 \end{bmatrix} \in \mathbb{R}^{3\times 3}.$$

$\|u\|$, with $u \in \mathbb{R}^n$, denotes the 2-norm of vector u. If $B \in \mathbb{R}^{n\times n}$, $\|B\|$ denotes the induced matrix 2-norm, i.e. $\|B\| = \max\{\|Bv\| : v \in \mathbb{R}^n \text{ with } \|v\| = 1\}$. The open ball of radius $\epsilon > 0$, centered at $x \in \mathbb{R}^n$ is defined as $B_\epsilon(x) = \{z \in \mathbb{R}^2 : ||z - x|| < \epsilon\}$, while the corresponding closed ball is defined as $\bar{B}_\epsilon(x) = \{z \in \mathbb{R}^2 : ||z - x|| \leq \epsilon\}$. In the paper we denote the complement of $B_\epsilon(x)$ in $\mathbb{R}^2$ by $(B_\epsilon(x))^c$. The boundary of a set A is defined as $\partial A = \bar{A} \setminus A^o$ where $\bar{A}$ is the closure of A

and A^o is its interior. If $A \subset \mathbb{R}^2$ we denote by $-A$ the set defined as $-A := \{x \in \mathbb{R}^2 : -x \in A\}$.

II. Formation Control Problem (FCP)

In this section the spacecraft model and all the assumptions related to the spacecraft's configuration are presented. The Formation Control Problem (FCP) is then formulated and it is shown that FCP can be cast as an equilibrium stabilization problem.

A. Model and Problem Statement

Consider two spacecraft under the gravitational influence of N massive bodies of the Solar System. In this paper, the superscript $(\cdot)^i$ is used to refer to the i-th spacecraft. Let $\mathcal{I}$ denote an inertial reference frame and let $\mathcal{B}^i = \{e_1^i, e_2^i, e_3^i\}$ denote the body frame of the i-th spacecraft, for $i = 1,2$. The rotation matrix of frame $\mathcal{I}$ with respect to frame $\mathcal{B}^i$ is denoted by R_i. We assume initially that the attitude of spacecraft 2 with respect to frame $\mathcal{I}$ is constant and we denote it by $\bar{R}_2$. In Section V, this assumption is relaxed and a robustness analysis is presented when R_2 varies with time, but remains in a small neighborhood of its nominal reference value $\bar{R}_2$. Let $X^i = (x_1^i, x_2^i, x_3^i)$ and $V^i = (x_4^i, x_5^i, x_6^i)$ denote the position and velocity of spacecraft i with respect to Earth, expressed in frame $\mathcal{I}$, for $i = 1,2$. The state vector of each spacecraft is taken to be $\chi^i := (X^i, V^i) \in \mathbb{R}^6$. Let $r^{j,1}(t)$ be the position vector of planet j with respect to Earth, expressed in the reference frame $\mathcal{I}$. The leader, spacecraft 1, is assumed to be unactuated and it follows a natural trajectory, while the follower is fully actuated. We denote by $u^2 = (u_1^2, u_2^2, u_3^2)$ the follower's control accelerations expressed in $\mathcal{B}^2$, generated by on-board thrusters. The equations of motion of the two spacecraft are

$$\begin{array}{ll} \dot{X}^1 = V^1 & \dot{X}^2 = V^2 \\ \dot{V}^1 = G^1(\chi^1, t), & \dot{V}^2 = G^2(\chi^2, t) + \bar{R}_2 u^2, \end{array} \tag{1}$$

where

$$G^i(\chi^i, t) = F^i(\chi^i, t) + H^i(\chi^i, t).$$

In the above, $F^i(\chi^i, t)$ models the effects of the gravitational fields of N planets on the i-th spacecraft,

$$F^i(\chi^i, t) = -\mu_1 \frac{X^i}{||X^i||^3} + \sum_{j=2}^{N} \mu_j \left(\frac{r^{j,1}(t) - X^i}{||r^{j,1}(t) - X^i||^3} - \frac{r^{j,1}(t)}{||r^{j,1}(t)||^3} \right), \tag{2}$$

μ_j is the gravitational parameter of planet j, and $H^i(\chi^i, t)$ models all of the external disturbances acting on the spacecraft. The model in (1) is the standard set of relative equations of motion with respect to Earth for the n-body problem, formulated in frame $\mathcal{I}$ (EPHEM model, [4]).
It is assumed that the follower spacecraft (spacecraft 2) can measure only its relative position and velocity with respect to the leader in its own body frame, i.e. the quantities $\Delta X := \bar{R}_2^T \left(X^2 - X^1 \right)$ and $\frac{d}{dt}\Delta X := \bar{R}_2^T \left(V^2 - V^1 \right)$. It is assumed that the follower is equipped with six constant-thrust electric thrusters, each providing a control acceleration $\bar{\omega} > 0$. We assume that the thrusters are assembled in opposing pairs, each aligned with a different body axis, so as to provide full position actuation. With this assumption, we may express the control input of spacecraft 2 as

$$u^2 = \bar{\omega} \begin{pmatrix} \sigma_1 \\ \sigma_2 \\ \sigma_3 \end{pmatrix},$$

where $\sigma_k \in \{-1,0,+1\}$, for $k = 1,2,3$ represents the on-off state of each thruster pair.
We define the distance $d_F(t)$ between the two spacecraft at time t as

$$d_F(t) = \sqrt{(x_1^2 - x_1^1)^2 + (x_2^2 - x_2^1)^2 + (x_3^2 - x_3^1)^2}$$

and the angles $\alpha_F(t)$ and $\beta_F(t)$ (indicated in Figure 1) as $\alpha_F(t) := \sin^{-1}\left((x_3^2 - x_3^1)/d_F\right)$ and $\beta_F(t) := \tan^{-1}\left((x_2^2 - x_2^1)/(x_1^2 - x_1^1)\right)$. In the following, a formation configuration will be indicated using the triple $(d_F(t),\alpha_F(t),\beta_F(t))$. This paper investigates the problem of achieving formations of two spacecraft with prescribed triple $(\bar{d}_F(t),\bar{\alpha}_F(t),\bar{\beta}_F(t))$. Figure 1 illustrates such a formation configuration.

Formation Control Problem (FCP): Consider two spacecraft modeled as in (1). Consider a desired formation configuration $(\bar{d}_F(t),\bar{\alpha}_F(t),\bar{\beta}_F(t))$ with $\bar{d}_F(t),\bar{\alpha}_F(t),\bar{\beta}_F(t)$ being twice differentiable bounded functions with bounded first and second derivative. We denote the associated set of constant admissible tolerances $(\delta d_F,\delta\alpha_F,\delta\beta_F)$. Design the *on-off* thrusters' switching cycles, using only measurements of the relative position in body frame, $\Delta X = \bar{R}_2^T\left(X^2 - X^1\right)$ and relative velocity $\Delta\dot{X} = \bar{R}_2^T\left(V^2 - V^1\right)$ of the follower with respect to the leader, such that the distance between the two spacecraft and the orientation of the formation converge and remain within a neighborhood $(\bar{d}_F(t) \pm \delta d_F,\bar{\alpha}_F(t) \pm \delta\alpha_F,\bar{\beta}_F(t) \pm \delta\beta_F)$ of the desired formation configuration $(\bar{d}_F(t),\bar{\alpha}_F(t),\bar{\beta}_F(t))$, by switching the on-off state of each thruster with finite frequency.

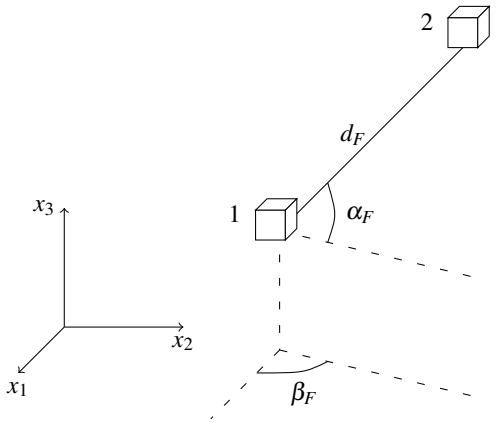

Fig. 1: Illustration of the formation configuration parameters $(d_F(t),\alpha_F(t),\beta_F(t))$.

The solution of FCP is derived in the ideal case of $R_2 = \bar{R}_2 = \text{const}$. A robustness analysis with respect to attitude perturbations is presented in Section V.

B. FCP as an equilibrium stabilization problem in relative coordinates

To solve FCP it is convenient to study the relative dynamics of the two spacecraft. Let $\hat{Z},\hat{V}$ be defined as

$$\begin{aligned} \hat{Z} &= \Delta X = \bar{R}_2^T\left(X^2 - X^1\right) \\ \hat{V} &= \Delta\dot{X} = \bar{R}_2^T\left(V^2 - V^1\right) \end{aligned} \tag{3}$$

Stabilizing the formation $(\bar{d}_F(t),\bar{\alpha}_F(t),\bar{\beta}_F)(t)$ is equivalent to stabilizing the relative state $(Z^\star(t),V^\star(t)) = (\bar{R}_2^T\bar{Z},\bar{R}_2^T\dot{\bar{Z}})$, where

$$\bar{Z}(t) = (\bar{d}_F(t)\cos(\bar{\alpha}_F(t))\cos(\bar{\beta}_F(t)),\bar{d}_F(t)\cos(\bar{\alpha}_F(t))\sin(\bar{\beta}_F(t)),\bar{d}_F(t)\sin(\bar{\alpha}_F(t))).$$

Consider the error coordinates

$$\begin{aligned} Z &= \hat{Z} - Z^\star(t) \\ V &= \hat{V} - V^\star(t). \end{aligned} \tag{4}$$

The error dynamics are

$$\begin{aligned} \dot{Z} &= V \\ \dot{V} &= D(Z,V,\chi^1,t) + u^2, \end{aligned} \tag{5}$$

where

$$D(Z,V,\chi^1,t) = -\dot{V}^\star(t) + \bar{R}_2^T\left(G^2(\chi^2,t) - G^1(\chi^1,t)\right).$$

Since G^1 and G^2 are bounded functions (if a neighborhood of the planets' centers is excluded) and $\dot{V}^\star(t)$ is bounded, we have that $D(Z,V,\chi^1,t)$ is bounded. Without any loss in generality, $D(Z,V,\chi^1,t)$ can be seen an exogenous, time dependent signal $D(t) = (d_1(t),$
$d_2(t),d_3(t))$ bounded by a positive constant $\bar{d}$. Note that stabilizing the origin of system (5) is equivalent to stabilizing the formation configuration $(\bar{d}_F(t),\bar{\alpha}_F(t),\bar{\beta}_F(t))$. System (5) can be rewritten as follows

$$\begin{aligned} \dot{z}_1 &= z_4 \\ \dot{z}_4 &= d_1(t) + \bar{\omega}\sigma_1 \\ \dot{z}_2 &= z_5 \\ \dot{z}_5 &= d_2(t) + \bar{\omega}\sigma_2 \\ \dot{z}_3 &= z_6 \\ \dot{z}_6 &= d_3(t) + \bar{\omega}\sigma_3, \end{aligned} \tag{6}$$

where σ_j is the control input, $j = 1,2,3$. System (6) can be thought of as a unit point-mass under the effect of a time-varying acceleration field $D(t)$. The point-mass in question is fully actuated with on-off inputs of magnitude $\bar{\omega}$ along three mutually orthogonal directions. Note that $z = (Z,V)$ is available for feedback. Since the three double integrators are formally decoupled, the desired formation configuration can be achieved by designing a stabilizer of the origin for the subsystem

$$\begin{aligned} \dot{x}_1 &= x_2 \\ \dot{x}_2 &= d(t) + \bar{\omega}\sigma, \end{aligned} \tag{7}$$

with control input σ having values in $\{-1,0,+1\}$, and using such controller in each of the subsystems of (6). In the following the solution of system (7) with initial conditions x_0 at t_0 is denoted by $\phi(t,t_0,x_0)$. We denote the class of piecewise continuous functions $d:\mathbb{R}\to\mathbb{R}$ by $\mathcal{U}$. In light of these observations, FCP can be reformulated as follows.

Revised FCP (RFCP): Consider system (7) with control input σ. Assume that $d(\cdot)\in\mathcal{U}$ is a function bounded by $\bar{d} > 0$, i.e. for all $t \geq 0$, $0 \leq |d(t)| \leq \bar{d}$. For a given control magnitude $\bar{\omega} > 0$, design a feedback controller with values in $\{-1,\ 0,\ +1\}$ such that

(i) The point $x = 0$ is *globally practically stable* (see [14]), i.e., for all $r > 0$ there exist controller parameters such that for all $x_0 \in \mathbb{R}^2$ and for all $t_0 \in \mathbb{R}$ there exists $T > 0$ such that $\phi(t,t_0,x_0) \in B_r(0)$ for all $t \geq T$,

(ii) given any compact time interval $[t_0,t_1]$, σ switches value a finite number of times.

It must be noted that while specification (i) is related to a stability property that the controller is required to enforce, specification (ii) follows from practical considerations related to the nature of the on-board thrusters. Given the type of electric thrusters on the spacecraft, we must avoid any high frequency switching behaviour. The control system must then be able to reach and stay in a desired neighborhood of the formation configuration, switching only a finite number of times over any compact interval of time.

III. Development

In this section the basic intuition leading to the solution of RFCP is presented. It is useful to first study the case with $d(t) \equiv 0$. Consider the double integrator

$$\begin{aligned} \dot{x}_1 &= x_2 \\ \dot{x}_2 &= \bar{\omega}\sigma, \end{aligned} \tag{8}$$

with states $x = (x_1, x_2) \in \mathbb{R}^2$, and let $\bar{\omega} > 0$ be fixed. Consider the problem of stabilizing the origin of system (8) by designing a switching function σ with values in the set $\{-1, 0, +1\}$. One obvious solution to this problem is the time-optimal control law (see, e.g., [15], [16])

$$\sigma = \begin{cases} -1, & x \in \Gamma^+ \\ +1, & x \in \Gamma^- \\ 0, & x = 0 \end{cases} \tag{9}$$

where Γ^+ and Γ^- are defined as (see Figure 2(a))

$$\begin{aligned} \Gamma^+ &= \{(x_1, x_2) \in \mathbb{R}^2 : x_1 > 0,\ x_2 > -\sqrt{2\bar{\omega}x_1}\} \cup \{(x_1, x_2) \in \mathbb{R}^2 : x_1 < 0,\ x_2 \geq \sqrt{-2\bar{\omega}x_1}\}, \\ \Gamma^- &= \{(x_1, x_2) \in \mathbb{R}^2 : x_1 > 0,\ x_2 \leq -\sqrt{2\bar{\omega}x_1}\} \cup \{(x_1, x_2) \in \mathbb{R}^2 : x_1 < 0,\ x_2 < \sqrt{-2\bar{\omega}x_1}\}. \end{aligned}$$

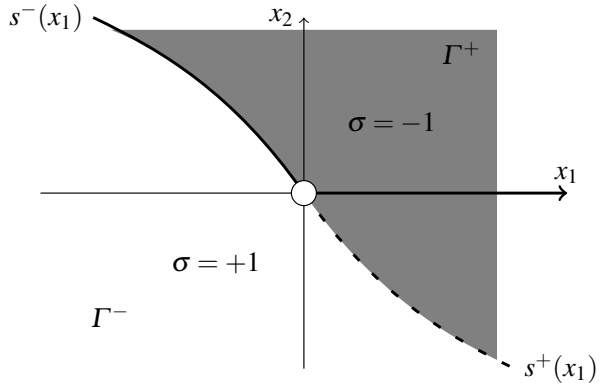

(a) Illustration of the sets Γ^+ and Γ^-.

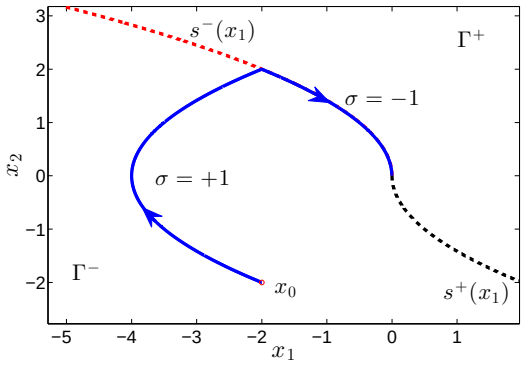

(b) Optimal solution starting at x_0.

Fig. 2: Time optimal controller for double integrators.

The definition of sets Γ^+ and Γ^- follows directly from the original solution of the time-optimal control problem for double integrators, see [15]. The parabola-shaped boundaries follow from the fact that solutions of system (8) with controller (9) are given by concatenations of arcs of

parabolas.The switching boundary is the set $\{(x_1,x_2)\in\mathbb{R}^2 : x_2 = -\text{sign}(x_1)\sqrt{2\bar{\omega}|x_1|}\}$. It is useful to define the two branches of the switching boundary using the two parametrizations:

$$s^+ : \mathbb{R}_{>0} \to \mathbb{R}^2, \quad s^+(x) = \left(x, -\sqrt{2\bar{\omega}x}\right), \qquad s^- : \mathbb{R}_{<0} \to \mathbb{R}^2, \quad s^-(x) = \left(x, \sqrt{-2\bar{\omega}x}\right).$$

Controller (9) globally stabilizes the origin in finite time with only one switch. Figure 2(b) shows an example of a state trajectory converging to the origin in finite time under controller (9). The state trajectories between switching points are arcs of parabolas. It is now shown that the time optimal controller (9) violates requirement (ii) of RFCP when applied to system (7). Return to the perturbed double-integrator (7), and suppose $d(t) \equiv -\bar{d}$, with $\bar{\omega} > \bar{d} > 0$. Let $x_0 = s^+(x_{01}) \in \Gamma^-$ for some $x_{01} \in \mathbb{R}_{>0}$, so that $\sigma = +1$. Referring to Figure 3(a), the state trajectory hits Γ^+ in finite time, inducing a switch to $\sigma = -1$. Since $d(t) \equiv -\bar{d}$, after an arbitrarily small interval of time, $\phi(t, t_0, x_0)$ enters Γ^- again, inducing a new switch to $\sigma = +1$. This process continues indefinitely, inducing a sliding mode along the switching curve $s^-(x_1)$ (i.e. the state trajectory is forced by the controller to slide along curve $s^-(x_1)$ by means of an infinite number of switchings), as shown in Figure 3(b) (only an approximate representation of the sliding mode can be obtained through simulation).

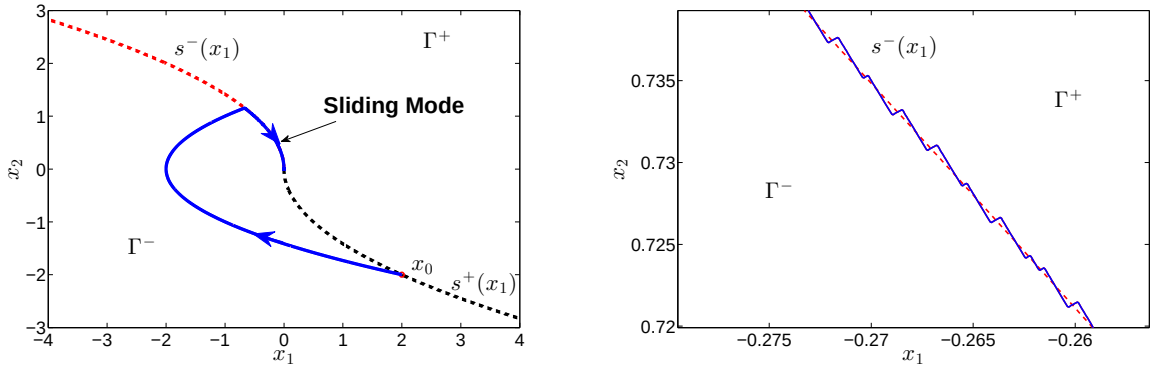

(a) A state trajectory of system (7) when $d(t) \equiv -\bar{d}$ and σ is given by (9).

(b) Zoom around the sliding mode. This is an illustration of the fact that the time optimal controller (9) violates requirement (ii) of RFCP.

Fig. 3: Sliding mode insurgence.

Despite the fact that sliding modes could be instrumental in stabilizing the origin, this condition is highly undesirable, since it would induce an infinite number of switchings on any compact time interval. Controller (9) must be modified in order to avoid sliding modes. Consider, as above, $x_0 = s^+(x_{01})$. A possible modification consists of disabling switching curve $s^+(x_1)$ once it has been hit, therefore allowing a switch if and only if the state trajectory hits the other switching parabola, $s^-(x_1)$. Although this eliminates sliding modes, it results in a loss of stability. Consider again the case $d(t) \equiv -\bar{d}$. The state trajectory through $x_0 = s^+(x_{01})$, hits the next switching curve in finite time, eventually diverging to infinity after the switch (Figure 4).
It has been shown so far that, in order to avoid infinitely many switchings, simply disabling a switching curve until another one is reached is not desirable, in that it gives a controller with

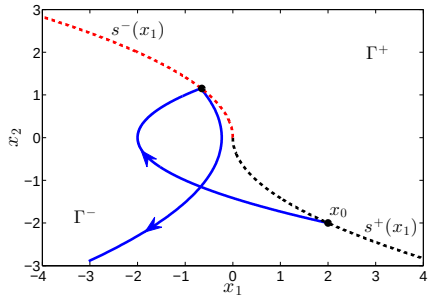

Fig. 4: Loss of stability with $d(t) \equiv -\bar{d}$.

no robustness to bounded disturbances. Further modifications are needed. Referring to Figure 5, two new switching sets are introduced:

$$\begin{aligned}\Lambda^+ &= \{(x_1,x_2) : x_1 \leq 0,\ x_2 \leq 0\} \cup \{(x_1,x_2) : x_1 > 0,\ x_2 \leq s^+(x_1)\},\\ \Lambda^- &= \{(x_1,x_2) : x_1 \geq 0,\ x_2 \geq 0\} \cup \{(x_1,x_2) : x_1 < 0,\ x_2 \geq s^-(x_1)\}.\end{aligned} \tag{10}$$

Note that the boundary of sets Λ^+ and Λ^- are given by sets

$$\partial\Lambda^+ = S^+ \cup \{(x_1,0) : x_1 \leq 0\}, \qquad \partial\Lambda^- = S^- \cup \{(x_1,0) : x_1 \geq 0\} \tag{11}$$

where

$$S^+ = \{s^+(x_1) : x_1 \in \mathbb{R}_{>0}\}, \qquad S^- = \{s^-(x_1) : x_1 \in \mathbb{R}_{<0}\}.$$

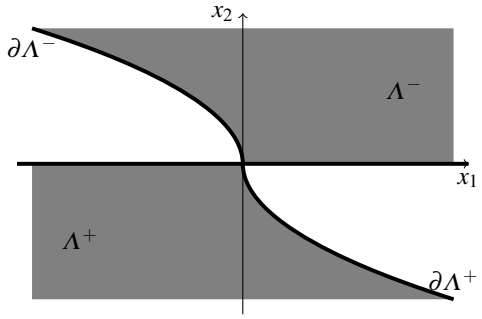

Fig. 5: Switching sets Λ^- and Λ^+.

The controller discussed in the following activates and deactivates the switching sets Λ^+ and Λ^- by means of a discrete variable q. The gap between Λ^+ and Λ^- (white region) guarantees that when trajectories are away from the origin, the switching frequency is bounded. Near the origin, the boundedness of the switching frequency is guaranteed by a basic hysteresis mechanism implemented using two nested balls $\bar{B}_{\delta_1}(0) \subset B_{\delta_2}(0)$. Moreover, with this choice of Λ^+ and Λ^-, if $d(t) \equiv 0$ then by setting $\delta_1 = \delta_2 = 0$ controller 12 reduces to the time-optimal bang-bang controller for the double integrator. We show in the next section that this control strategy is robust against bounded disturbances and avoids infinite switchings, therefore solving RFCP.

IV. Solution of RFCP

In this section we present a feedback controller[1] solving RFCP, and present a proof of its convergence properties.

A. Control Law

The intuition presented above can be formalized by a hybrid control law. The introduction of discrete states q_j allows us to activate and deactivate the switching sets Λ^+, Λ^-. Let $r > \delta_2 > \delta_1 > 0$ be design parameters, where $r > 0$ is the radius of the neighborhood that has to be stabilized, δ_1 is the radius of the open ball in which the controller is turned off, and δ_2 is the radius of the ball outside which the controller is turned on again.

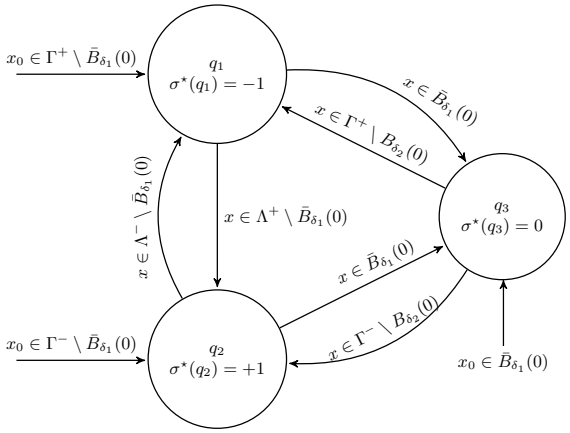

Fig. 6: Finite state machine representing the proposed controller.

The control law is described by the finite state machine in Figure 6, characterized by discrete states $Q = \{q_1, q_2, q_3\}$, continuous states $x \in \mathbb{R}^2$ and hybrid feedback $\sigma^\star(\cdot) : Q \to \mathbb{R}$ with

$$\begin{aligned} \sigma^\star(q_1) &= -1 \\ \sigma^\star(q_2) &= +1 \\ \sigma^\star(q_3) &= 0. \end{aligned} \tag{12}$$

In the following, the state transitions from state q_j to state q_k, with $k \neq j$, will be denoted by $q_j \to q_k$. Referring to Figure 6, if $x_0 \in \Gamma^+ \setminus \bar{B}_{\delta_1}(0)$ the discrete state is initialized at q_1 and, therefore, the control value is $\sigma^\star(q_1) = -1$. The only allowable state transition from q_1 occurs either when $x(t)$ enters $\bar{B}_{\delta_1}(0)$ ($q_1 \to q_3$), in which case the control value is switched to $\sigma^\star(q_3) = 0$, or when $x(t)$ enters $\Lambda^+ \setminus \bar{B}_{\delta_1}(0)$, ($q_1 \to q_2$), in which case σ is switched to $\sigma^\star(q_2) = +1$. Therefore the switching set Λ^- is disabled when the discrete state is at q_1. Similarly, in q_2 the switching set Λ^+ is disabled and the control value can only switch when the state enters $\bar{B}_{\delta_1}(0)$ or when it enters set $\Lambda^- \setminus \bar{B}_{\delta_1}(0)$. In q_3, the controller is turned off, and it will be turned on only when the state exits $B_{\delta_2}(0)$. In particular, the control value will be switched to $+1$ when $x(t)$ enters $\Gamma^- \setminus B_{\delta_2}(0)$ ($q_3 \to q_2$), and to -1 when $x(t)$ enters $\Gamma^+ \setminus B_{\delta_2}(0)$, ($q_3 \to q_1$).

[1]The controller discussed in this section is also discussed in the conference proceedings [13].

In a mutually exclusive manner, the finite state machine in Figure 6, by means of the discrete states $\{q_1, q_2, q_3\}$, enables and disables the switching sets and regulates the hysteresis of the controller near the origin. If δ_1, δ_2 are picked sufficiently small, the state trajectory enters $B_r(0)$ in finite time and never leaves it.

Theorem IV.1 Controller (12) solves RFCP if the thrust magnitude $\bar{\omega}$ satisfies the condition $\bar{\omega} > \bar{d}/2\left(1+\sqrt{5}\right)$. In particular, if this inequality holds, then for any $r > 0$ there exist scalars δ_1, δ_2 with $0 < \delta_1 < \delta_2 < r$, such that for all solutions through x_0 there is $T_{x_0} > 0$ such that $x(t) \in B_r(0)$ for all $t \geq T_{x_0}$.

Remark IV.2 *: It is possible to show that the conditions of Theorem IV.1 are also necessary, not just sufficient, but this is beyond the scope of this paper.*

B. Preliminaries

In the remaining part of the section we present the proof of Theorem IV.1. We begin with some preliminary results. Fix an initial condition x_0 and an automaton state q_j with $j \in \{1,2\}$.

Definition IV.3 The **attainable set** $\mathcal{A}^{q_j}(x_0,t)$ **from** x_0 **at time** t of system (7) is the set

$$\mathcal{A}^{q_j}(x_0,t) = \{x(t) : \text{there exists } d \in \mathcal{U} \text{ such that } x(t) \text{ is a solution of (7) through } x_0 \text{ with perturbation } d(t) \text{ and } \sigma = \sigma^\star(q_j)\}.$$

The **attainable set** $\mathcal{A}^{q_j}(x_0)$ **from** x_0 is the set $\mathcal{A}^{q_j}(x_0) = \bigcup_{t\geq 0} \mathcal{A}^{q_j}(x_0,t)$. △

It is shown in [17] that the boundary of the attainable set $\mathcal{A}^{q_j}(x_0)$ from x_0 of a certain class of planar nonlinear systems is a union of phase curves of two special differential equations, the so-called extremal vector fields. Their solutions are denoted $\phi_L^{q_j}(t,x_0)$ and $\phi_R^{q_j}(t,x_0)$. We refer to [17] for the details on how to construct $\phi_L^{q_j}(t,x_0)$, $\phi_R^{q_j}(t,x_0)$. Given $q_j \in Q$, curves $\phi_L^{q_j}(s,x_0)$ and $\phi_R^{q_j}(s,x_0)$ are the curves of maximum and minimum acceleration, for all the admissible $d(t) \in \mathcal{U}$. It naturally follows that $\phi_L^{q_j}(s,x_0)$ and $\phi_R^{q_j}(s,x_0)$ form the boundary of the attainable set $\mathcal{A}^{q_j}(x_0)$. In the case of system (7), by applying the results in [17], the extremal solutions can be computed analytically and are concatenations of arcs of parabolas defined as

$$X_s^{q_j}(x_0) = \begin{bmatrix} \left(-\bar{d} + (-1)^j\bar{\omega}\right)\frac{s^2}{2} + x_{02}s + x_{01} \\ \left(-\bar{d} + (-1)^j\bar{\omega}\right)s + x_{02} \end{bmatrix} \quad Y_s^{q_j}(x_0) = \begin{bmatrix} \left(\bar{d} + (-1)^j\bar{\omega}\right)\frac{s^2}{2} + x_{02}s + x_{01} \\ \left(\bar{d} + (-1)^j\bar{\omega}\right)s + x_{02} \end{bmatrix},$$

with $j \in \{1,2\}$, where j refers to the index of the current value of the automaton state, q_j. The concatenation occurs when the solution hits $\{x_2 = 0\}$. More precisely, for all $x_0 \in \mathcal{R}^- = \{x \in \mathbb{R}^2 : x_2 < 0\}$ (with $\mathcal{R}^+ = \{x \in \mathbb{R}^2 : x_2 > 0\}$), $\phi_L^{q_j}(s,x_0)$, $\phi_R^{q_j}(s,x_0)$ are given by

$$\phi_L^{q_j}(s,x_0) = \begin{cases} Y_s^{q_j}(x_0), & \text{if } Y_s^{q_j}(x_0) \in \mathcal{R}^- \\ X^{q_j}_{s-s_Y^j(x_0)} \circ Y^{q_j}_{s_Y^j(x_0)}(x_0), & \text{if } Y_s^{q_j}(x_0) \in \mathcal{R}^+ \end{cases} \tag{13}$$

$$\phi_R^{q_j}(s,x_0) = \begin{cases} X_s^{q_j}(x_0), & \text{if } X_s^{q_j}(x_0) \in \mathcal{R}^- \\ Y^{q_j}_{s-s_X^j(x_0)} \circ X^{q_j}_{s_X^j(x_0)}(x_0), & \text{if } X_s^{q_j}(x_0) \in \mathcal{R}^+, \end{cases} \tag{14}$$

where $s_X^j(x_0) = -\dfrac{x_{02}}{(-1)^j\bar{\omega}-\bar{d}}$, $s_Y^j(x_0) = -\dfrac{x_{02}}{(-1)^j\bar{\omega}+\bar{d}}$. If $x_0 \in \mathcal{R}^+$ the extremal curves are defined equivalently by substituting $X_s^{q_j}(x_0)$ with $Y_s^{q_j}(x_0)$, s_X^j with s_Y^j and vice versa in (13) and (14) (we refer to [17] for an extensive treatment of extremal vector fields of planar non linear systems). Using this fact we prove that the first discrete transition $q_j \to q_k$, with $j,k \in \{1,2,3\}$, exists for all $x_0 \in \mathbb{R}^2$ if $\bar{\omega} > \bar{d}$.

Lemma IV.4 Let $0 < \delta_1 < \delta_2$. If $\bar{\omega} > \bar{d}$, then for all $x_0 \in (\bar{B}_{\delta_1}(0))^c$ and all $d \in \mathcal{U}$, there exists a finite $\tau > 0$ such that $q_j \to q_k$ when $t = \tau$, for some $j,k \in \{1,2,3\}$, $k \neq j$.

Proof: Suppose $\bar{\omega} > \bar{d}$ and let, without loss of generality, $x_0 \in \Gamma^- \setminus \bar{B}_{\delta_1}(0)$. Controller (12) is initialized at q_2, with $\sigma = \sigma^\star(q_2) = +1$. Set $\mathcal{A}^{q_2}(x_0)$ is represented in Figure 7. Note that $\mathcal{A}^{q_2}(x_0)$ is bounded. Suppose, by way of contradiction, that for some $d \in \mathcal{U}$, the solution $x(t)$ of (7) with initial condition x_0 and $\sigma = \sigma^\star(q_2) = +1$ does not enter the set $\Lambda^- \cup \bar{B}_{\delta_1}(0)$. Therefore $x(t)$ must remain in the shaded region of Figure 7 for all $t \geq 0$. However, the inequality $\dot{x}_2 = d(t) + \bar{\omega} \geq \bar{\omega} - \bar{d} > 0$ implies that the solution $x(t)$ is unbounded, which gives a contradiction.

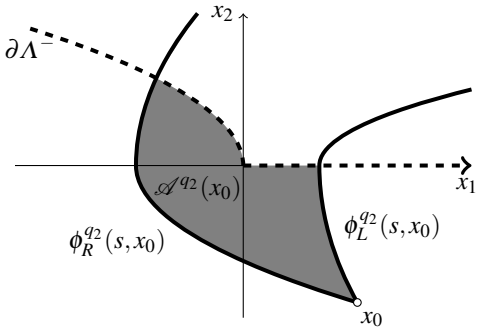

Fig. 7: Attainable set from x_0, $\mathcal{A}^{q_2}(x_0)$. The shaded region indicates the region accessible to $x(t)$ before inducing a discrete state transition $q_2 \to q_j$, $j \in \{1,3\}$.

□ ■

We propose in the following a formal definition of switching time and switching point.

Definition IV.5 Let $x(t)$ be a solution of system (7) with hybrid feedback (12). A time instant t_i, with $i \in \mathbb{N}$, is called a **switching time** if $x(t_i) \in \left(S^+ \cup S^- \cup \bar{B}_{\delta_1}(0)\right)$ and at time $t = t_i$ a state transition $q_j \to q_k$, with $j,k \in \{1,2,3\}$, $j \neq k$ occurs. The value of the state at a switching time, $x^i = x(t_i)$ is called a **switching point**. △

The definition of switching point allows us to investigate the types of state trajectories induced by controller (12). Consider, without loss of generality, $x^i \in S^+$. By Lemma IV.4 the state trajectory will either hit the switching set Λ^- on S^- or on the x_1-axis. If the trajectory hits Λ^- on S^-, then, by Definition IV.5, switching point $x^{i+1} \in S^-$ is defined. This situation is depicted in Figure 8(a) and is referred to as 1-switch. If, on the other hand, the trajectory hits Λ^- on the x_1-axis, one can show, by applying Lemma IV.4 with the new control value $\sigma = \sigma^\star(q_1) = -1$, that the state trajectory must later hit the active switching set Λ^+ on S^+, inducing switching point $x^{i+1} \in S^+$. This situation is depicted in Figure 8(b) and is referred to as 2-switch. If $x(t)$ enters $\bar{B}_{\delta_1}(0)$, then

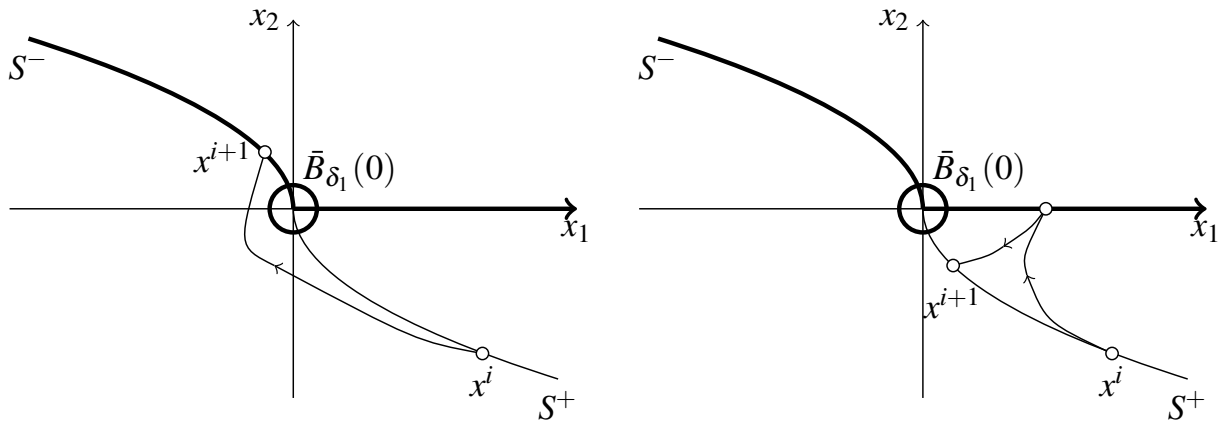

(a) 1-Switch. The state trajectory starts from $x^i \in S^+$ and hits set Λ^- on S^-.

(b) 2-Switch. The state trajectory starts from $x^i \in S^+$, hits Λ^- on the positive x_1 axis and returns to set Λ^+ on S^+.

Fig. 8: Types of switching points induced by hybrid feedback (12).

switching point $x^{i+1} \in \bar{B}_{\delta_1}(0)$ is denoted 0-switch. One can show that these are the only possible trajectories induced by controller (12).

To summarize, if $\bar{\omega} > \bar{d}$, only three types of switching points are possible (see Figure 8).

- x^{i+1} is a **1-switch from** x^i, if one of x^i or x^{i+1} belongs to S^+, and the other one belongs to S^-.
- x^{i+1} is a **2-switch from** x^i, if both x^i, x^{i+1} belong to the same arc of parabola, S^+ or S^-.
- x^{i+1} is a **0-switch from** x^i, if $x^{i+1} \in \bar{B}_{\delta_1}(0)$.

By Lemma IV.4, if $\bar{\omega} > \bar{d}$, then controller (12) induces a sequence of switching points $\{x^i\}_{i\in I}$, with $i \in I \subset \mathbb{N}$ nonempty, such that $\left(x^1, \ldots, x^i \in (\bar{B}_{\delta_1}(0))^c\right) \Rightarrow i+1 \in I$. We now show that the sequence of switching points converge to the origin if $\bar{\omega} > \bar{d}(1+\sqrt{5})/2$, by showing that the sequence $\{||x^i||\}_{i\in I}$ contracts. In particular, we show that if $x^i, x^{i+1} \in (\bar{B}_{\delta_1}(0))^c, ||x^{i+1}|| \leq \bar{\alpha}||x^i||$, for some $0 < \bar{\alpha} < 1$.

Consider the intersection of the attainable set $\mathcal{A}^{q_j}(x^i)$ from $x^i \in S^+$ with the active switching set $\Lambda^- \cup \bar{B}_{\delta_1}(0)$ and let p, v be defined as in Figure 9.

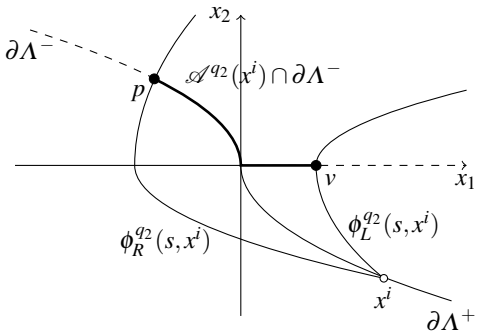

Fig. 9: Attainable switching set from x^i.

If $x(t)$ performs a 1-Switch, $x^{i+1} \in \mathcal{A}^{q_2}(x^i) \cap \partial\Lambda^-$, and therefore $||x^{i+1}|| \leq ||p||$. By using the analytic form of $\phi_R^{q_2}(s,x^i)$ in (13), one can show that $p_1 = -\alpha_1^2 x_1^i$ where $\alpha_1^2 = \left(\bar{d}(\bar{d}+\bar{\omega})\right) / \left((\bar{\omega}-\bar{d})(2\bar{\omega}+\bar{d})\right)$. This implies that $||x^{i+1}|| \leq ||p|| \leq \alpha_1 ||x^i||$. If $\bar{\omega} > \bar{d}(1+\sqrt{5})/2$, then $\alpha_1 < 1$. If, on the other hand, $x(t)$ performs a 2-switch, $|x_1^{i+1}| \leq |v_1|$, since $\mathcal{A}^{q_1}(v)$ is delimited by parabolas with negative concavity from v. By using the analytic expression of $\phi_L^{q_2}(s,x^i)$, one can show that $|v_1| = \alpha_2^2 |x_1^i|$, where $\alpha_2^2 = \left(1 - \bar{u}/(\bar{u}+\bar{f})\right)$. If $\bar{\omega} > \bar{d}(1+\sqrt{5})/2$, then $\alpha_2 < 1$ and $||x^{i+1}|| \leq \alpha_2 ||x^i||$. Therefore if $\bar{\omega} > \bar{d}(1+\sqrt{5})/2$, then $||x^{i+1}|| \leq \bar{\alpha} ||x^i||$, with $\bar{\alpha} = \max\{\alpha_1, \alpha_2\} < 1$.
We have proved the following result.

Lemma IV.6 Consider system (7) with hybrid feedback (12), and pick δ_1, δ_2 such that $0 < \delta_1 < \delta_2$. If $\bar{\omega} > \bar{d}\left(1+\sqrt{5}\right)/2$, there exists $\bar{\alpha} \in (0,1)$ such that for any $d \in \mathcal{U}$ and any initial condition, the sequence $\{x^i\}_{i\in I}$ of switching points induced by the solution $x(t)$ of (7) with hybrid feedback (12) is contracting as long as $x^i \notin \bar{B}_{\delta_1}(0)$.

Lemma IV.6 implies that the sequence $\{x^i\}_{i\in I}$ converges to $\bar{B}_{\delta_1}(0)$ and so for all $x_0 \in \mathbb{R}^2$ and for all $\delta_2 > 0$ there exists $T_{x_0} \geq 0$ such that $x(T_{x_0}) \in \bar{B}_{\delta_2}(0)$. The following lemma shows that for all $r > 0$, one can pick $\delta_1 < \delta_2 < r$ so that, after entering $B_{\delta_2}(0)$, $x(t)$ remains in $B_r(0)$, switching with finite frequency.

Lemma IV.7 Consider system (7) with the hybrid feedback (12). For any $r > 0$ there exist δ_1, δ_2, $0 < \delta_1 < \delta_2 < r$, and a compact positively invariant set $\mathcal{Q}$ such that $\bar{B}_{\delta_2}(0) \subset \mathcal{Q} \subset B_r(0)$.

Proof: Let $\mathcal{P}_i$ be the compact region depicted in Figure 10, delimited by the extremal solutions $\phi_R^{q_2}(s,x^i)$, $\phi_L^{q_2}(s,x^i)$, and by $\partial\Lambda^-$. Let $\mathcal{Q}^i = \mathcal{P}_i \cup -\mathcal{P}_i$. Extremal solutions $\phi_L^{q_2}(s,x^i)$,

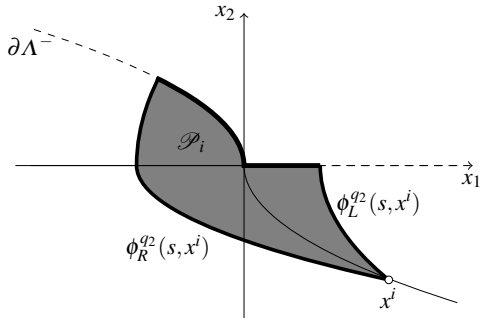

Fig. 10: Set $\mathcal{P}_i$.

$\phi_R^{q_2}(s,x^i)$ have the property [17] that all solutions of (7) with $\sigma = \sigma^\star(q_j)$ cross the curve $\phi_L^{q_2}$ to the left, and $\phi_R^{q_2}$ to the right. Therefore solutions in $\mathcal{P}_i$ can only exit it through $\partial\Lambda^-$. Since $\mathcal{P}_i \cap \partial\Lambda^- \subset -\mathcal{P}_i$ and $-\mathcal{P}_i \cap \partial\Lambda^+ \subset \mathcal{P}^i$, it follows that $\mathcal{Q}_i$ is positively invariant. One can readily see that there exists $c > 0$ such that, for all i, $\mathcal{Q}_i \subset B_{c\|x^i\|}(0)$. Since the sequence $\{x^i\}_{i\in I}$ is contracting, there exists $i \in I$ such that $c\|x^i\| < r$, so that $\mathcal{Q}_i \subset B_r(0)$. Clearly $0 \in \text{int}\mathcal{Q}_i$ so there exists $\delta_2 > 0$ such that $\bar{B}_{\delta_2}(0) \subset \text{int}\mathcal{Q}_i$. $\delta_2 > 0$ can be computed as follows. If $(\bar{\omega}-\bar{d})^2 + \bar{\omega}\bar{d} - \bar{d}\sqrt{\bar{\omega}^2 + c^2 r^2} < 0$ then pick $\delta_2 < \sqrt{2\bar{d}(-\bar{\omega} + \sqrt{\bar{\omega}^2 + c^2 r^2}) - (\bar{\omega}-\bar{d})^2}$, otherwise pick $\delta_2 < |\frac{-\bar{d}}{\bar{\omega}-\bar{d}}(-\bar{\omega} + \sqrt{\bar{\omega}^2 + c^2 r^2})|$, where $c = \min\{1, \left((\bar{\omega}-\bar{d})^2/\bar{d}^2 + 2\bar{\omega}(\bar{\omega}-\bar{d})/(r\bar{d})\right)^{\frac{1}{2}}\}$. Next, pick $\delta_1 \in (0, \delta_2)$. The choice of δ_1 affects

only the frequency of the controller near the origin. The positive invariance of $\mathcal{Q}_i$ is preserved with these choices of δ_1, δ_2 because $\bar{B}_{\delta_2}(0) \cap \partial\mathcal{Q}_i = \varnothing$. ■

□

Remark IV.8 *The conditions on the admissible value of δ_2 are only sufficient. As such, they can be very conservative when considering practical applications, increasing the switching frequency of the controller. One can adjust the value of δ_2 by a simple trial and error process.*

C. Proof of Theorem IV.1

We are now ready to prove the main result of the paper.

Proof: For any $r > 0$, by Lemma IV.7 there exists a positively invariant set $\mathcal{Q}$ and $0 < \delta_1 < \delta_2$ such that $\bar{B}_{\delta_2} \subset \mathcal{Q} \subset B_r(0)$. For any initial condition in $(\bar{B}_{\delta_1}(0))^c$ and any $d \in \mathcal{U}$, the solution $x(t)$ gives rise to a well-defined switching sequence $\{x^i\}_{i\in I}$. By Lemma IV.6, this sequence is contracting as long as $x^i \notin \bar{B}_{\delta_1}(0)$. Since $\bar{B}_{\delta_1}(0) \subset \bar{B}_{\delta_2}(0) \subset \mathcal{Q}$, $x^i \in \mathcal{Q}$ for sufficiently large i. By Lemma IV.7, $x(t) \in \mathcal{Q} \subset B_r(0)$ for all $t \geq t_i$.

■

□

V. Robustness to Attitude Perturbations

In this section we study the robustness of controller (12) with respect to perturbations on the attitude of the follower spacecraft. The results presented in this section are twofold. We first show that, by choosing $\bar{\omega}$ according to Theorem IV.1, controller (12) solves FCP if the perturbation on the follower's attitude is small enough. We then show that, if the performances of the attitude control system are known, $\bar{\omega}$ can be chosen so as to compensate the perturbations acting on the spacecraft. Suppose that, according to Theorem IV.1, $\bar{\omega}$ has been chosen so that $\bar{\omega} = \lambda\bar{d}(1+\sqrt{5})/2$, with $\lambda > 1$. Suppose that the attitude of the follower is perturbed around its target configuration $\bar{R}_2$. Let $\theta_1, \theta_2, \theta_3$ denote the angles associated with the $1-2-3$ Euler angle sequence. Let $\bar{\theta}_1, \bar{\theta}_2, \bar{\theta}_3$ be the angles associated with the target spacecraft orientation $\bar{R}_2$ (assuming, without loss of generality that the reference configuration does not correspond to the singularity of the Euler representation). Under the assumption of small attitude perturbations, the rotation of the follower can be linearized and written as

$$R_2(t) \approx (1_3 - \delta\psi(t)^\times)\bar{R}_2 \tag{15}$$

where 1_3 is the 3×3 identity matrix and $\delta\psi(t) = S(\bar{\theta}_2, \bar{\theta}_3)\delta\theta(t)$ with

$$S(\bar{\theta}_2, \bar{\theta}_3) = \begin{bmatrix} \cos\bar{\theta}_2\cos\bar{\theta}_3 & \sin\bar{\theta}_3 & 0 \\ -\cos\bar{\theta}_2\sin\bar{\theta}_3 & \cos\bar{\theta}_3 & 0 \\ \sin\bar{\theta}_2 & 0 & 1 \end{bmatrix}.$$

The vector $\delta\theta(t) = [\delta\theta_1(t)\ \delta\theta_2(t)\ \delta\theta_3(t)]$ denotes the perturbations on each angle of the Euler sequence. The equations of motion of the follower can be rewritten as

$$\begin{aligned} \dot{X}^2 &= V^2 \\ \dot{V}^2 &= G^2(\chi^2, t) + (1_3 - \delta\psi(t)^\times)\bar{R}_2 u^2(t), \end{aligned} \tag{16}$$

Consider the coordinate transformation proposed in (3) and (4)

$$\begin{aligned} Z &= \bar{R}_2^T\left(X^2 - X^1\right) - Z^\star(t) \\ V &= \bar{R}_2^T\left(V^2 - V^1\right) - V^\star(t) \end{aligned} \tag{17}$$

Note that $\bar{R}_2$ is constant. Z, V are no longer the relative position and relative velocity between the two spacecraft expressed in frame $\mathcal{B}^2$. Z, V must be estimated by the spacecraft. By applying such coordinate transformation to (16), the error dynamics can be rewritten as

$$\begin{aligned} \dot{Z} &= V \\ \dot{V} &= \tilde{D}(t) + u^2(t), \end{aligned} \tag{18}$$

where

$$\tilde{D}(t) = D(t) - \bar{R}_2^T \delta\psi(t)^\times \bar{R}_2 u^2(t). \tag{19}$$

As in Section II-B, stabilizing the origin of system (18) is equivalent to stabilizing the desired formation configuration. The function $\tilde{D}(t)$ is bounded. The dependence of $\tilde{D}(t)$ by $u(t)$ does not prevent us from applying the results of Theorem IV.1, since $\tilde{D}(t)$ is still a time-varying bounded function in $\mathcal{U}$. We are interested in finding a bound on the attitude perturbation $\delta\theta(t)$ so that, whenever the follower's attitude is kept inside such bound, controller (12) still meets its control objectives.

$$\begin{aligned} ||\tilde{D}(t)|| &\leq \bar{d} + \|\bar{R}_2^T \delta\psi(t)^\times \bar{R}_2 u^2(t)\| \leq \bar{d} + \|\bar{R}_2^T (\bar{R}_2 u^2(t))^\times \delta\psi(t)\| \\ &\leq \bar{d} + \|(u^2(t))^\times \bar{R}_2^T S(\bar{\theta}_2, \bar{\theta}_3)\| \|\delta\theta(t)\| \leq \bar{d} + \|(u^2(t))^\times\| \|S(\bar{\theta}_2, \bar{\theta}_3)\| \|\delta\theta(t)\|. \end{aligned}$$

It can be easily shown that $\|(u^2(t))^\times\| \leq \sqrt{3}\,\bar{\omega}$ and $\|S(\bar{\theta}_2, \bar{\theta}_3)\| = \sqrt{1 + |\sin\bar{\theta}_2|}$. Therefore

$$\|\tilde{D}(t)\| \leq \bar{d} + \sqrt{3}\,\bar{\omega} \left(\sqrt{1 + |\sin\bar{\theta}_2|} \right) \|\delta\theta(t)\|. \tag{20}$$

By Theorem IV.1, if $\bar{\omega} > \|\tilde{D}(t)\| \left(1 + \sqrt{5}\right)/2$ then controller (12) solves RFCP. If

$$\bar{\omega} > \left(\bar{d} + \sqrt{3}\,\bar{\omega} \left(\sqrt{1 + |\sin\bar{\theta}_2|} \right) \|\delta\theta(t)\| \right) \left(1 + \sqrt{5}\right)/2 \tag{21}$$

then the condition required by Theorem IV.1 is satisfied. By using the fact that $\bar{\omega} = \lambda \bar{d}(1 + \sqrt{5})/2$ the bound on the attitude perturbation $\delta\theta$ can be easily computed as

$$\|\delta\theta(t)\| < \frac{2(\lambda - 1)}{\lambda\sqrt{3}\left(1 + \sqrt{5}\right)\sqrt{1 + |\sin\bar{\theta}_2|}}. \tag{22}$$

As long as the follower's orientation satisfies the bounds given by condition (22), controller (12) successfully achieves the control objectives. Suppose, on the other hand, that we are given the maximum orientation error allowed by the on-board attitude control system, denoted by $\|\delta\theta\|_{\max}$. If $\|\delta\theta\|_{\max} < 2/\left(\sqrt{3}(1 + \sqrt{5})\sqrt{1 + |\sin\bar{\theta}_2|}\right)$, relation (21) can be used to find the value of $\bar{\omega}$ that allows to reject the disturbance and achieve the main control specifications

$$\bar{\omega} > \frac{\bar{d}\left(1 + \sqrt{5}\right)}{2 - \sqrt{3}\left(1 + \sqrt{5}\right)\left(\sqrt{1 + |\sin\bar{\theta}_2|}\right)\|\delta\theta\|_{\max}}. \tag{23}$$

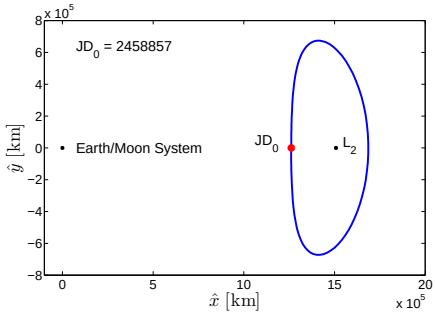

Fig. 11: Nominal Halo orbit in the Sun-Earth/Moon system, as seen in the classical Sun-Earth rotating frame.

VI. Simulations

In this section we present some simulation results in order to prove the effectiveness of controller (12). Let $m_1 = m_2 = 400\,\text{kg}$ be the mass of the two spacecraft. The leader is not controlled and follows a Halo orbit around the libration point L_2 of the Sun-Earth/Moon system, Figure 11. We assume here as inertial frame $\mathcal{I}$ an ecliptic frame centered at the Sun. The dynamics of the two vehicles is modeled as in (1), the motion of the Sun and the Earth/Moon system is assumed to be circular while the gravitational perturbations of all the planets have been considered.
It is assumed that the follower (spacecraft 2) is fully actuated with a total of 6 electric thrusters providing a constant thrust of $\bar{T} = 40\mu N$ each. We consider a case of practical interest for interferometric missions: we assume the target configuration to be described by constant triple $(200\,\text{m}, \frac{\pi}{9}, \frac{\pi}{6})$. This triple describes a fixed formation in $\mathcal{I}$ that allows the cluster to perform the observation of a fixed target. We assume that the attitude of the follower with respect to frame $\mathcal{I}$ is constant and given by the rotation matrix:

$$R = \begin{bmatrix} -0.2988 & -0.5794 & -0.7583 \\ -0.9543 & 0.1814 & 0.2374 \\ 0 & 0.7946 & -0.6072 \end{bmatrix}$$

As shown in Section II-B, this last assumption is not essential, in that a time varying orientation would result only in additional disturbance terms, easily compensated by feedback 12. For these simulations it was assumed that the spacecraft have access to the exact value of their relative position and velocity.
The simulated scenario is similar to the mission profile of the SI mission [1]: three control phases are defined in the following, characterized by increasingly tighter tolerances on d_F, α_F and β_F.

- **Phase 1** (rough control): $(\ \delta d_F,\ \ \delta\alpha_F,\ \ \delta\beta_F\ ) = (\ 1\,\text{m},\ \ 0.017\,\text{rad},\ \ 0.017\,\text{rad}\ )$
- **Phase 2** (intermediate control): $(\ \delta d_F,\ \ \delta\alpha_F,\ \ \delta\beta_F\ ) = (\ 10\,\text{cm},\ \ 0.0017\,\text{rad},\ \ 0.0017\,\text{rad}\ )$
- **Phase 3** (fine control): $(\ \delta d_F,\ \ \delta\alpha_F,\ \ \delta\beta_F\ ) = (\ 1\,\text{mm},\ \ 5\cdot 10^{-6}\,\text{rad},\ \ 5\cdot 10^{-6}\,\text{rad}\ )$

The scenario has been simulated for a total time interval of $T = 16$ days. Note that open balls $B_{r_i}(0)$ can be substituted with open boxes U_i^j defined as $U_i^j = \left(-\delta z_i^j, \delta z_i^j\right) \times \left(-\delta z_{i+3}^j, \delta z_{i+3}^j\right)$, where δz_i^j refers to the tolerance for state z_i during phase j. Equivalently, balls $B_{\delta_1}(0)$ and $B_{\delta_1}(0)$ have been replaced by boxes. As mentioned in Remark IV.8, their size has been adjusted by trial and error.

TABLE I: Components of sets U_i^j for each phase of the mission.

Tolerance	Phase 1	Phase 2	Phase 3
δz_1	0.7281 m	0.0728 m	$6.81 \cdot 10^{-4}$ m
δz_2	1.0018 m	0.1002 m	$6.918 \cdot 10^{-4}$ m
δz_3	0.7179 m	0.0718 m	$6.859 \cdot 10^{-4}$ m
δz_4	$3 \cdot 10^{-4}$ m/s	$1 \cdot 10^{-4}$ m/s	$1 \cdot 10^{-5}$ m/s
δz_5	$3 \cdot 10^{-4}$ m/s	$1 \cdot 10^{-4}$ m/s	$1 \cdot 10^{-5}$ m/s
δz_6	$3 \cdot 10^{-4}$ m/s	$1 \cdot 10^{-4}$ m/s	$1 \cdot 10^{-5}$ m/s

The relative initial conditions have been assumed to be $\hat{Z}_0 = \bar{R}_2^T(-5, 5, 5)$ m and $\hat{V}_0 = \bar{R}_2^T(-1.2 \cdot 10^{-3}, 2 \cdot 10^{-3}, 10^{-4})$ m/s. Figure 12(a) presents the approaching phase to the desired neighborhood of $(200, \frac{\pi}{9}, \frac{\pi}{6})$ in the phase plane of the subsystem $z_1 - z_4$. Note that the state trajectory closely resembles the original undisturbed case, thanks to the low intensity of the gravity differential between the two spacecraft. Figures 12(b), 13(a) and 13(b) present a magnification of the behaviour of the state trajectory in the selected neighborhoods, during each phase of the mission, for subsystem $z_1 - z_4$. As the figures suggest, the proposed controller successfully keeps the state trajectory inside the target sets. Equivalent results are obtained for subsystems $z_2 - z_5$ and $z_3 - z_6$.

As can be seen in Figure 14(a), the distance between the two spacecraft approaches a neighborhood of the target configuration. Figures 14(b) to 17(b) confirm that not only the pair of spacecraft approaches the nominal configuration $(\bar{d}_F, \bar{\alpha}_F, \bar{\beta}_F)$, but also that during each phase of the mission, after short transients, the corresponding tolerance bounds are satisfied. Moreover, it must be stressed that the only limit to the level of accuracy achievable by controller (12) is given by the accuracy of the on-board sensors and by the maximum on-off frequency sustainable by the selected thrusters. Figure 19(a) presents the *on-off* switching function for one of the thrusters of the follower spacecraft over the entire simulation interval. Figure 19(b) presents the switching history for phase 3 of the simulation. The other five thrusters present similar switching histories. They are therefore not shown here. Note from Figures (19(a)) and (19(b)) that feedback (12) turns on and off each thruster with finite frequency. Indeed, as Figure 19(b) shows, under tight tolerance requirements each correction maneuver lasts for a few minutes while the time between two successive activations of the thruster is of the order of one hour.

Figures 12(a) to 17(a) show that controller (12), successfully achieves and keeps the desired formation configuration meeting the specified tolerance limits, by means of a total of 6 *constant thrust* electric thrusters. In the worst case scenario (no intervals with thrusters off), the total cost of the mission would be of approximately $\Delta v = 4.66$ m/s over a timespan of 180 days (the period of the Halo orbit). The cost is then very limited, especially considering that such a Δv is to be obtained using electric thrusters. Recent developments in the field of FEEP propulsion systems, as in [18], showed that similar performances can be obtained with just few grams of propellant.

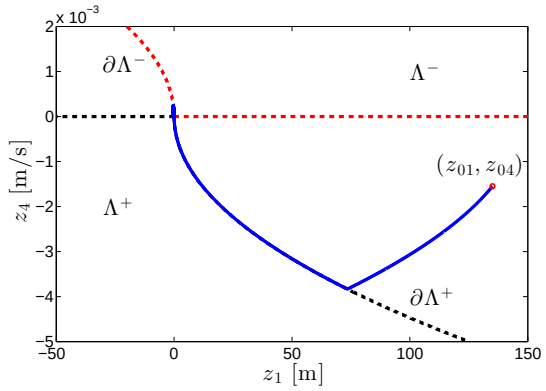

(a) (z_1, z_4) subsystem. The state trajectory approaches a neighborhood of the origin.

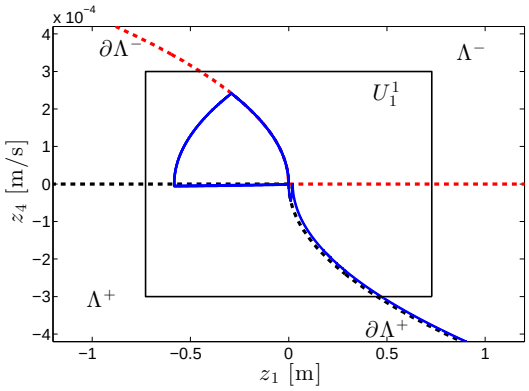

(b) Formation keeping for phase 1. The state is successfully kept inside the target set.

Fig. 12: Phase 1.

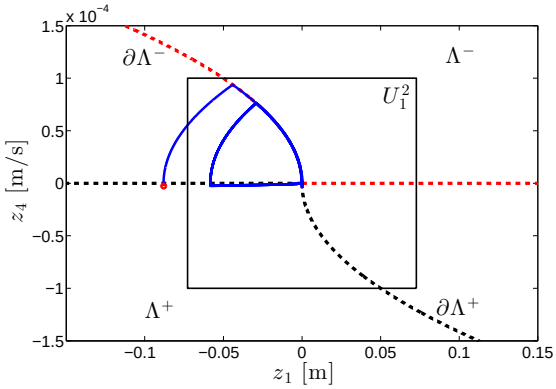

(a) Formation keeping for phase 2. The state is successfully kept inside the target set.

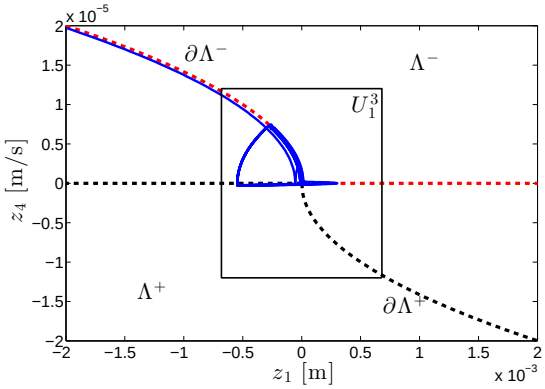

(b) Formation keeping for phase 3. The state is successfully kept inside the target set.

Fig. 13: Phases 2 and 3.

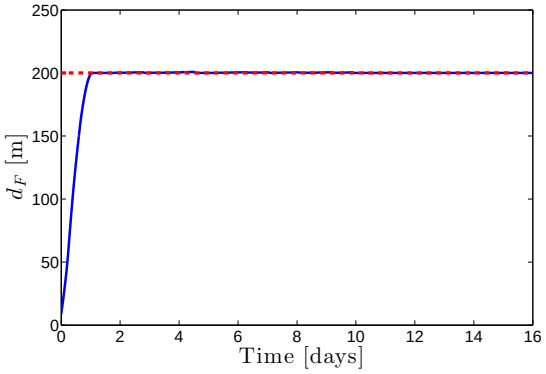

(a) The distance between the spacecraft approaches a neighborhood of $\bar{d}_F$.

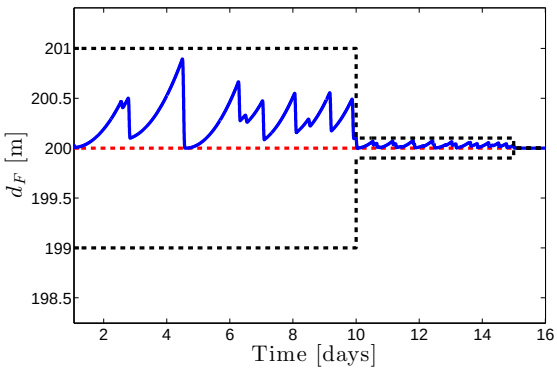

(b) After short transients, $d_F(t)$ is kept, during each phase, inside the desired bounds.

Fig. 14: Distance between the spacecraft $d_F(t)$.

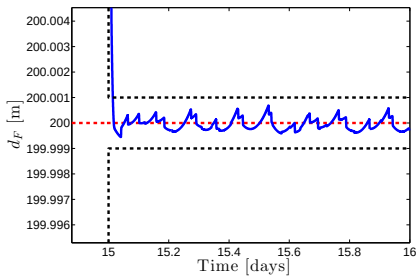

Fig. 15: After a short transient, $d_F(t)$ is kept in the target bound of phase 3.

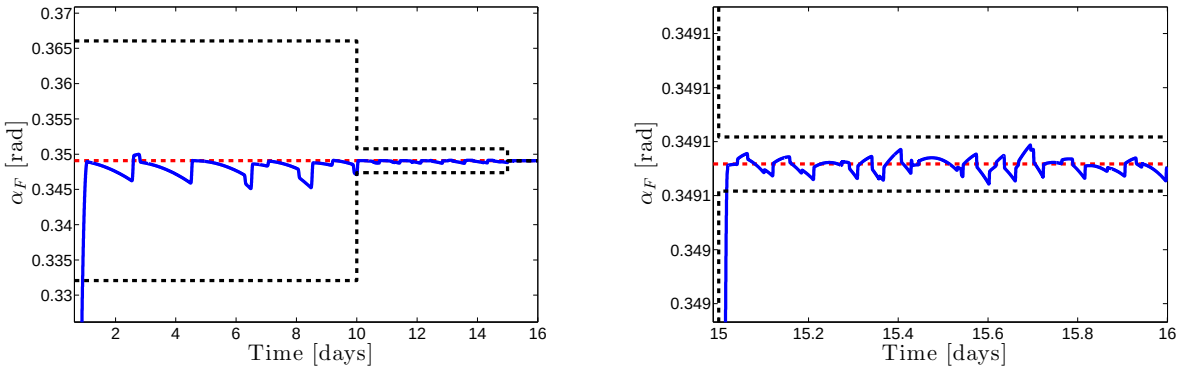

(a) After short transients, $\alpha_F(t)$ is kept, during each phase, inside the desired bounds.

(b) After a short transient, $\alpha_F(t)$ is kept in the target bound of phase 3.

Fig. 16: Angle between the spacecraft $\alpha_F(t)$.

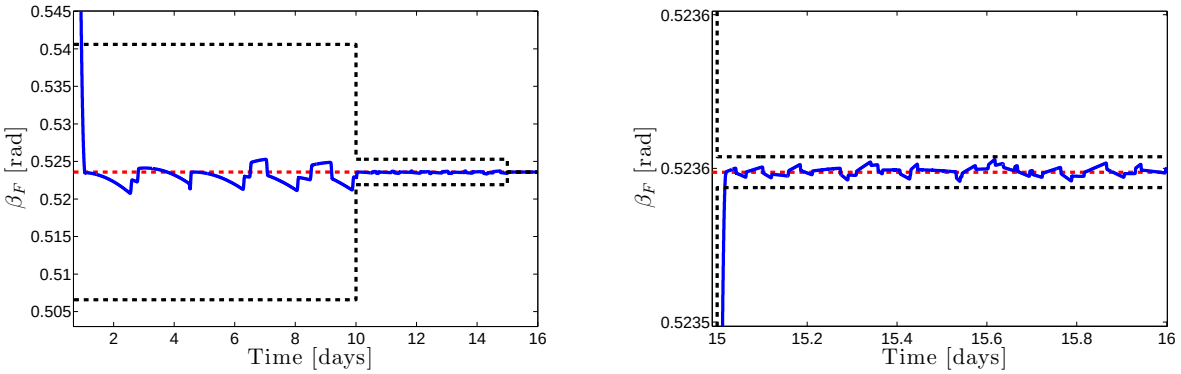

(a) After short transients, $\beta_F(t)$ is kept, during each phase, inside the desired bounds.

(b) After a short transient, $\beta_F(t)$ is kept in the target bound of phase 3.

Fig. 17: Angle between the spacecraft $\beta_F(t)$.

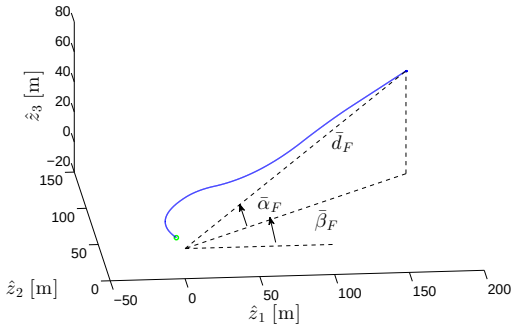

Fig. 18: Trajectory of the follower spacecraft seen by the leader.

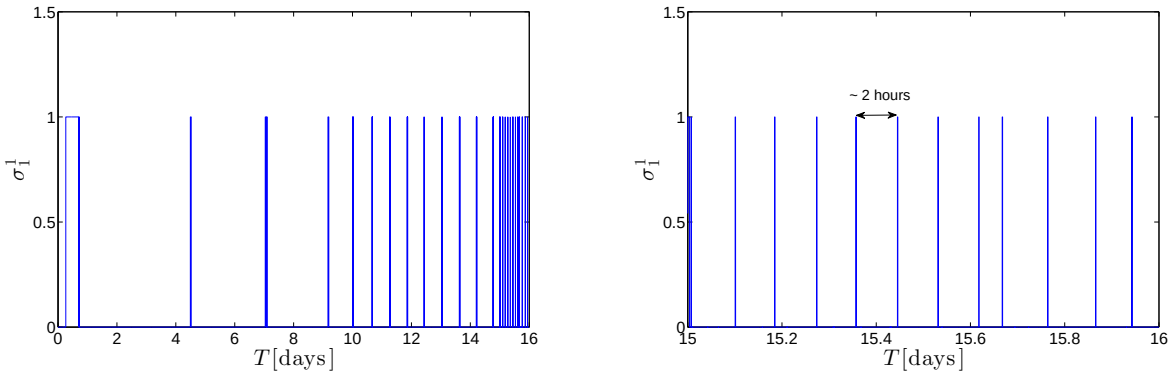

(a) On-off switching function, phases 1 and 2.

(b) On-off switching function, phase 3.

Fig. 19: Switching function for thruster 1.

VII. Conclusions

The paper introduces a new hybrid controller for the stabilization of spacecraft formations flying in the vicinity of the L_2 libration point of the Sun-Earth/Moon system, by using on-off electric thrusters. Such a controller permits the achievement and maintenance of the formation meeting any tolerance level on the formation's length and orientation (sufficient conditions on the thrust magnitude are provided). This is obtained by properly coordinating the on-off cycles of the on board thrusters. By design the controller is robust to bounded unmodeled disturbances.

References

[1] Carpenter, K. G., Schrijver, C. J. and Karovska, M.: The stellar imager (SI) vision mission. In: Proceedings of the SPIE 6268, Advances in Stellar Interferometry (2006)

[2] Coulter, Daniel R.: NASA's Terrestrial Planet Finder mission: the search for habitable planets. In: Proceedings of the SPIE 5487, Optical, Infrared, and Millimeter Space Telescopes (2003)

[3] Gendreau, K. C., Cash, W. C., Shipley, A. F., and White, N.: MAXIM Pathfinder x-ray interferometry mission. In: Proceedings of the SPIE 4851, X-Ray and Gamma-Ray Telescopes and Instruments for Astronomy (2003)

[4] Howell, K.C., and Marchand, B. G.: Natural and Non-Natural Spacecraft Formations Near the L_1 and L_2 Libration Points in the Sun–Earth/Moon Ephemeris System. Dynam. Syst. **20**(1), 149-173 (2005)
[5] Millard, L.D., and Howell, K. C.: Control of Interferometric Spacecraft Arrays for (u, v) Plane Coverage in Multi-Body Regimes. J. Astronaut. Sci. **56**(1), 71-97 (2008)
[6] Qi, R., Xu, S., and Xu, M.: Impulsive Control for Formation Flight About Libration Points. J. Guid. Control Dyn. **35**(2), 484-496 (2012)
[7] Marchand, B.G., and Howell, K.: Control Strategies for Formation Flight in the Vicinity of the Libration Points. J. Guid. Control Dyn. **28**(6), 1210-1219 (2005)
[8] Gurfil, P., and Kasdin, N. J.: Stability and Control of Spacecraft Formation Flying in Trajectories of the Restricted Three-Body Problem. Acta Astronaut. **54**(6), 433-453 (2004)
[9] Gurfil, P., Idan, M., and Kasdin, N. J.: Adaptive Neural Control of Deep-Space Formation Flying. J. Guid. Control Dyn. **26**(3), 491-501 (2003)
[10] Marchand, B.G. and Stanton, S.A.: Actuator Constrained Optimal Formation Keeping Near the Libration Points. J. Astronaut. Sci. **57**(3), 607-632 (2010)
[11] Stanton, S. A. and Marchand, B.: Actuator Constrained Optimal Control of Formations Near the Libration Points. AIAA/AAS Astrodynamics Specialist Conference, Honolulu, HI (2008)
[12] Serpelloni, E., Maggiore, M. and Damaren, C.J.: Achieving Rigid Spacecraft Formations Using Thrusters with One-Bit Resolution. AIAA/AAS Astrodynamics Specialist Conference, San Diego, CA (2014)
[13] Serpelloni, E., Maggiore, M. and Damaren, C.J.: Bang Bang Hybrid Stabilization of Perturbed Double Integrators. Proceedings of the 53^{rd} IEEE Conference on Decision and Control, Los Angeles, CA (2014)
[14] Chaillet, A., and Loria, A.: Uniform Global Practical Asymptotic Stability for Time-Varying Cascaded Systems. Automatica **12**(6), 595-605 (2006)
[15] Bryson, A. E., and Ho, Y.: Applied Optimal Control: Optimization, Estimation, and Control. Hemisphere, New York, 110-117 (1975)
[16] Rao, V.G., and Bernstein, D. S.: Naive Control of the Double Integrator. IEEE Control Syst. Mag. **21**(5), 86-97 (2001)
[17] Maggiore, M., Rawn, B., and Lehn, P.: Invariance Kernels of Single-Input Planar Nonlinear Systems. SIAM J. Control Optim. **50**(2), 1012-1037 (2012)
[18] Biagioni, L., Ceccanti, F., Saverdi, M., Saviozzi, M., and Andrenucci, M.: Qualification Status of the FEEP-150 Electric Micropropulsion Subsystem. AIAA Paper, 2005-4261 (2005)
[19] Folta, D., Hartman, K., Howell, K.C., and Marchand, B.: Formation Control of the MAXIM L_2 Libration Orbit Mission. AIAA Paper, 2004-5211 (2004)
[20] Goebel, R., Sanfelice, R. G., and Teel, A.: Hybrid Dynamical Systems. IEEE Control Syst. Mag. **29**(2), 28-93 (2009)
[21] Marcuccio, S., Genovese, A., and Andrenucci, M.: Experimental Performance of Field Emission Microthrusters. J. Propul. Power **14**(5), 774-781 (1998)